Investigation of the Melting Behavior and Morphology Development of Polymer Blends in the Melting Zone of Twin-Screw Extruders

H. POTENTE,[1] S. KRAWINKEL,[1] M. BASTIAN,[1] M. STEPHAN,[2] P. PÖTSCHKE[2]

[1] Institut für Kunststofftechnik, Universität Paderborn, 33098 Paderborn, Germany

[2] Institut für Polymerforschung, 01069 Dresden, Germany

Received 23 October 2000; accepted 21 February 2001

ABSTRACT: The melting behavior and the morphology development that runs parallel to it play central roles in the processing of polymer blends. We studied the impact of speed, melt throughput, continuous-phase viscosity, screw configuration, and disperse-phase content on the melting behavior and morphology development in the melting zone of a twin-screw extruder. The polymer blend used incorporated polyamide-6 (PA6) as its disperse phase and a high-viscosity or low-viscosity polypropylene as the matrix phase. The melting behavior of the polymer blend was investigated with press plates. A qualitative assessment was made of the processes, on basis of the optical impression gained from the transilluminated press plates. One key result was that the PA6 granules melted very rapidly in the polypropylene melt. We took samples over the length of the melting section to permit a quantitative assessment of the morphology. The results show a finely dispersed morphology already at the start of the melting section. This did not undergo any essential change as the blend passed through the extruder, and only a limited correlation was evident with the process parameters.
 J Appl Polym Sci 82: 1986–2002, 2001

Key words: blends; melting; morphology; press plate; breakup mechanisms

INTRODUCTION

Corotating, tightly intermeshing twin-screw extruders are the main type of extruder used for polymer compounding. The self-cleaning of the tightly intermeshing screw profile and the modular design of the screw and screw barrel have prompted widespread use of this design. The corotating twin-screw extruder serves two main functions on account of its efficient mixing properties. First, it is used to modify standard polymers that have fillers and additives incorporated into them during extrusion, and second, it is used for the production of an increasing number of polymer blends.[1,2] Because a number of key properties of polymer blends are conditioned by the phase morphology, greater insight is required into the process before it can be optimized. It is also known that significant changes in morphology occur during the melting process. Once melting is completed, only comparatively minor changes take place.[3–6,9] In view of this situation, a closer study must be made of the melting zone of corotating twin-screw extruders during blend processing.

Correspondence to: S. Krawinkel.
Contract grant sponsor: Deutsche Forschungsgemeinschaft.

Journal of Applied Polymer Science, Vol. 82, 1986–2002 (2001)

EXPERIMENTAL

Materials

Investigations were conducted into two blend systems based on polypropylene (PP) and polyamide-6 (PA6). The continuous phases studied were a low-viscosity PP grade (PPN; Novolen® 1100N, BASF-AG) and a high-viscosity PP grade (PPH; Novolen® 1100H, Targor GmbH). The disperse component was PA6 (Ultramid® B35, BASF AG), with weight contents of 5, 10, 20, and 30%. The blend systems were incompatible; in other words, the components remained separate in the blends. The selective solubility of the disperse phase made this material combination readily accessible in analytical terms.

The viscosity ratio (p) is defined as the quotient of the viscosities of the disperse phase (η_d) and matrix phase (η_m), as shown in Figure 1:

$$p = \frac{\eta_d}{\eta_m} \tag{1}$$

The p range is $0.3 < p < 3$ for the PPH/PA6 blend and $1.2 < p < 9$ for the PPN/PA6 blend in the relevant extruder shear rate range of approximately $1\ s^{-1} \leq \dot{\gamma} \leq 1000\ s^{-1}$ and at the standard processing temperatures. Results obtained by Grace[7] and later by Wu[8] show that p values of 0.1–1 are best for promoting drop breakup. With p values in excess of 1, they found an increase in the number-average diameter of the disperse particles as p increased. Under these conditions, the PPH/PA6 blend offers more favorable conditions for drop breakup.

Before the actual blending, PA6 was mixed in a drum mixer for 15 min with a Heliogen green K8734 pigment produced by BASF AG (Ludwigshafen, Germany). It was then compounded in a twin-screw extruder (TSE) and granulated. The pigmentation ensured a sufficient contrast between the disperse and matrix phases for evaluation by the press-plate method.

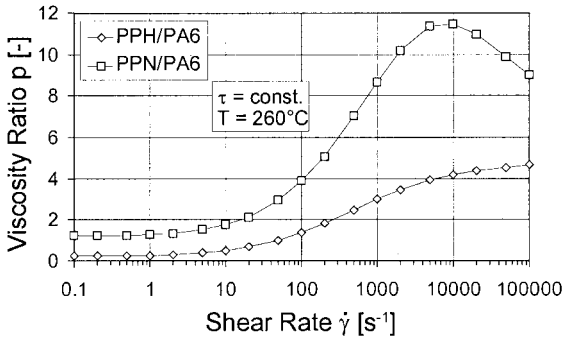

Figure 1 Viscosity ratio p for the blends.

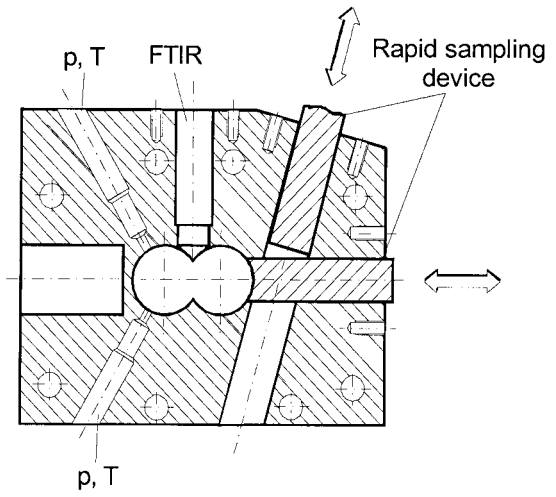

Figure 2 Picture of an SP.[9]

Machinery and Experimental Procedures

A corotating TSE ZSK40 from Krupp Werner & Pfleiderer was used for the study. So-called sample plates (SPs) were fitted to the melting section of the extruder so that the melting behavior and morphology development could be observed in the melting section. These removal devices took the form of intermediate housing plates, as shown in Figure 2, and permitted a sample of extrudate to be removed during the running process.[9,10]

Figure 3 shows the machine configuration and the position of the four SPs over the melting section.

The heatable barrels had a temperature of 260°C and the end plate of 255°C. We also fitted a flow restrictor at the end plate of the extruder to give a defined back-pressure length. We used the melt pressure at sample plate 1 (SP1) as the actuating variable to control the back-pressure behavior. This was necessary because the blend would not have melted fully with the nonheated SP and the smaller amount of heat introduced into the system. Two gravimetric weigh feeders metered the two blend components into the feed barrel from above. The PA6 granules were dried overnight (for ca. 8 h) around 80°C before processing. All the samples taken during the tests were removed during a steady-state extruder operation.

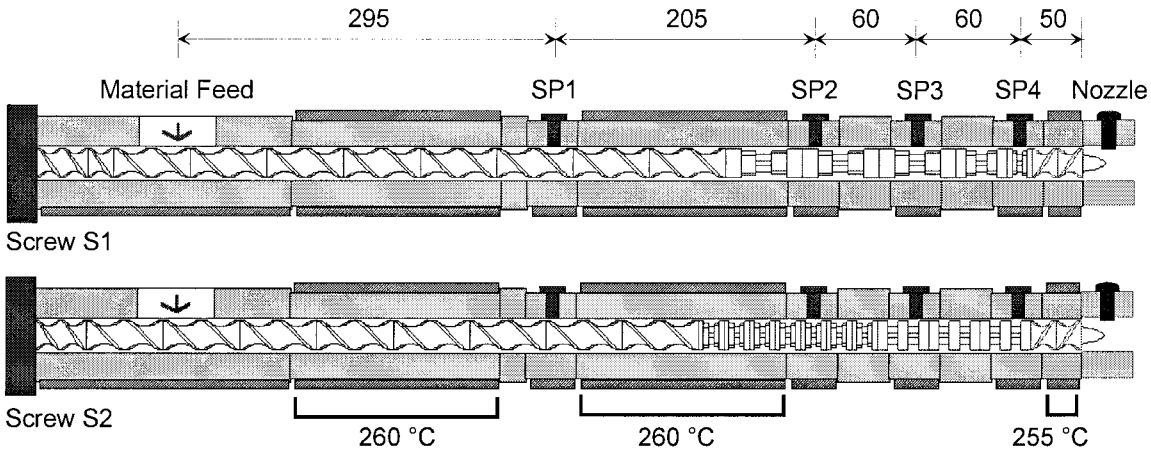

Figure 3 Machine configuration.

Preparation of the Press Plates

The melting behavior of the disperse PA6 phase was qualitatively assessed in this study with so-called press plates. This assessment involved a strand of melt being removed from the opened SP and subsequently being formed into a plate on a press. The press was heated to a press temperature (T_P) of 130°C [$T_P <$ melting temperature of PA6 ($T_{K,\mathrm{PA}}$) and melting temperature of PP ($T_{K,\mathrm{PP}}$)], and the melt strand was placed in a square frame with an inside length of 110 mm, generating a press-plate thickness of approximately 3 mm. After removal from the press, the press plate was cooled to room temperature in a water bath. Plates obtained in this way illustrate the melting behavior of the blend system. They were subsequently photographed with a digital camera with a cold-light source and saved as digital images for evaluation.

Preparation of the Samples

To permit quantification of the finely dispersed morphology inside the blends, we also took samples for microscopic study, in addition to the melt strands required to produce the press plates. A smaller sample approximately 5 mm in diameter and 8 mm long was cut with a cylindrical cutter tool and immediately cooled in liquid nitrogen ($T \approx -296$°C) to prevent any morphology changes. A sample could thus be taken from the melt strand and frozen within 5 s, with very little time left for microrheological and thermodynamic equilibrium processes. Figure 4 shows the aforementioned sample-removal operation in a schematic diagram.

To analyze the morphology, we cut the samples with a microtome (Leica Jung 2055 Autocut) with a glass blade, giving a flat study surface. We performed a quantitative analysis of the morphology by dissolving out the disperse phase with formic acid and achieving a contrast with the matrix phase. The etched samples were then studied with a scanning electron microscope (Leo 455VP, Zeiss; 10 kV). In the microscopic assessment, the smallest measurable particle size was approximately 0.15 μm with an enlargement (E) of 2000 and approximately 0.3 μm with an E value of 1000. The quantitative evaluation was performed on a personal computer with Optimas V5.23 image-processing software.

Strategy for the Separation of Dispersed Particles by Dissolution of the Matrix Phase

To examine the drop breakup mechanisms, we isolated the disperse PA6 particles by dissolving the PP matrix phase, and we made recordings with scanning electron microscopy. The solvent used was a mixture of diphenyl amine and xylene. Figure 5 shows a schematic diagram of the procedure employed.

Particle Size Measurement

The particle size distribution was determined from scanning electron micrographs of the cut and prepared sample surfaces with Optimas image-processing software. Particle size was determined with the equivalent circle diameter (ECD), which can be worked out with eq. (2):

$$\mathrm{ECD} = \sqrt{\frac{4}{\pi} \cdot (A_{\mathrm{Particle}})} \qquad (2)$$

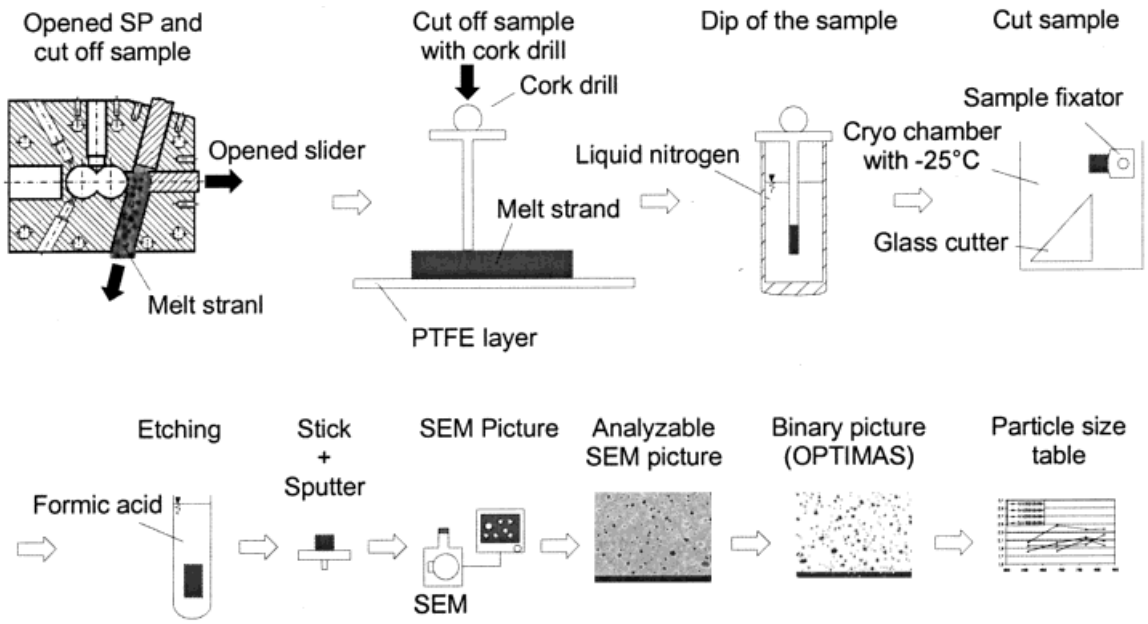

Figure 4 Preparation and analysis of the samples.

Because a large number of different-sized dispersed particles are seen when the morphology is quantified, two different mean values are calculated for the ECD to permit a more effective description:

$$\mathrm{ECD}_z = \frac{\sum \mathrm{ECD}_i}{n} \tag{3}$$

$$\mathrm{ECD}_v = \left(\frac{\sum \mathrm{ECD}_i^3}{n}\right)^{1/3} \tag{4}$$

Equation (3) describes the number-average particle diameter (ECD_Z). This differs from the volume-average particle diameter (ECD_V) in that all the size classes receive the same weighting. ECD_V from eq. (4) reacts considerably more sensitively

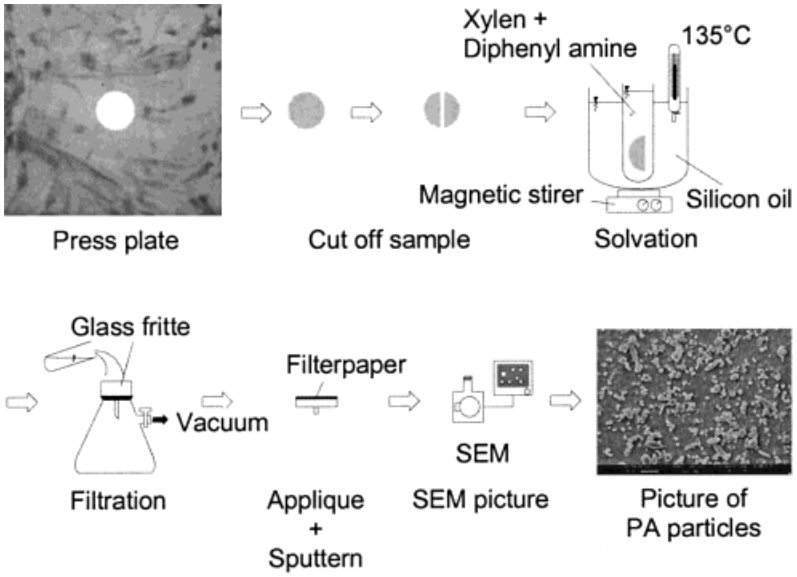

Figure 5 Strategy for the preparation of dispersed particles via dissolution of the matrix phase.

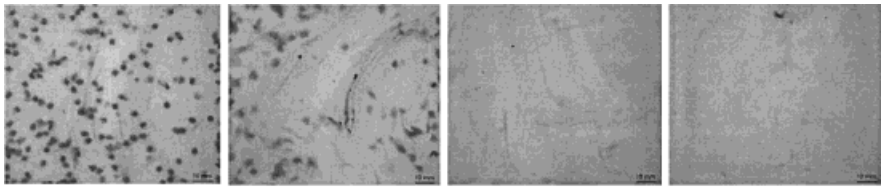

Figure 6 Press-plate series for demonstrating the melting behavior with screw S2, n_S = 200 min^{-1}, $\dot{m}$ = 30 kg/h, and w_{PPN} = 90%.

to changes in the number of big particles. This means that clear differences can result in a comparison with the number-average diameter over the length of a mixing section. The standard deviation (SD) of the ECDs that are established can be set out with the aid of eq. (5):

$$SD = \sqrt{\frac{1}{n-1}\sum_{i=1}^{n}(x_i - \bar{x})^2} \quad (5)$$

The SD is a measure of the scatter of the diameter values for the ECDs established.

RESULTS

Melting Behavior

The melting of pure polymers is described as a multistage process in the literature.[5,10–13] In the majority of cases, studies are conducted with transparent or folding barrels. A distinction is essentially drawn among four stages of granule melting behavior. At the start of melting, granules are heated in the conveying section through heat conduction and heat convection, undergoing slight deformation as they pass through the intermeshing zone of the screw. As melting progresses, heat is introduced via contact with the heated barrel wall, and a melt film also forms through the friction between the solid particles. At the same time, aggregates develop, caused by the contact between granules, which are surrounded by melt. In addition to this, dissipative heating can occur through particle deformation. At this point, the granules are already in the fully filled mixing section of the extruder, which is made up of kneading block elements. The granules melt completely in this section, as a result of thermal conduction, convection, and dissipation. On industrial screw configurations, partial filling (chamber conveyance) frequently prevails in the solid-conveying section, whereas the melting section is completely filled. This results in the granules being conveyed directly into the melt on account of their higher velocity.[13] Geng and Zhu[11] referred to this process as *mix-melting*.

Observed Phenomena

This model concept can also be used with certain restrictions for blend systems such as the PP/PA6 blend in this study. In this blend system, the disperse PA6 phase (T_K = 223°C) has a higher crystalline melting temperature than the PP matrix phase (T_K = 167°C). Because the disperse PA6 phase is starting to melt, the PA6 granules are, therefore, already surrounded by fully melted PP. It is clear from the press plates shown in Figure 6 for one of the test points examined in this study that the pigmented PA6 granules (dark spots) melt very rapidly.

At sample removal point SP2, the PA6 phase has only undergone slight melting. At the subsequent removal point SP3, the number of PA6 granules has clearly fallen. Granules with the same large diameters as at SP2 are still clearly evident here, however. This phenomenon can be explained by, among other things, the dissimilar residence times of the PA6 particles in the extruder melting zone. At the following removal point, SP4, no PA6 granules can be seen any more. The phenomena described on the basis of this press-plate series were seen with all the samples taken.

The observations show, therefore, that the PA6 pellets floating in the PP melt disappear very rapidly after their solid-to-liquid phase transition. An evaluation of the press plates also reveals no intermediate drop sizes after this phase transition. Instead, a type of definitive, finely dispersed blend morphology results from the liquid granule-like drops [granule diameter (d_G) $\approx$ 4

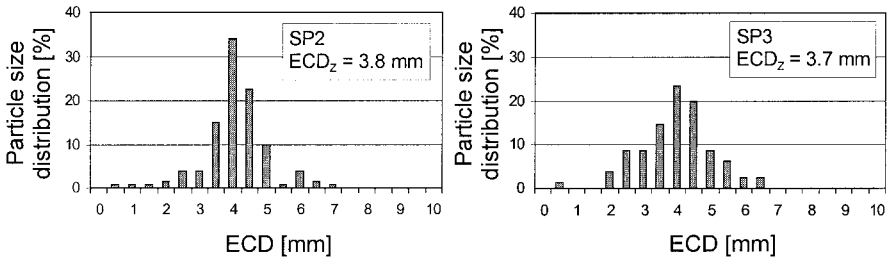

Figure 7 Particle size distribution of nonmolten PA6 granules with screw S2, n_S = 200 min^{-1}, $\dot{m}$ = 30 kg/h, and w_{PPN} = 90%.

mm] after just a short time. This then remains virtually unchanged during the remainder of the extrusion process. The change in the size distribution of the pigmented PA6 granules in the press plates is shown in Figure 7.

When the values of the mean ECDs are compared, they are seen to be almost identical. The mean ECD is 3.8 mm at SP2 and 3.7 mm at SP3. The granules have a starting diameter of d_G = 4.1 mm. The distribution curves also show that the first two press plates only contain granules virtually similar in diameter. Although the edge regions of the curves also display a certain proportion of bigger and smaller granules compared with the mean ECD, this is due primarily to the error in quantifying the superimposed granules, which are spread over several planes of the press plates. This also explains why a number of particle sizes in excess of the starting d_G were measured.

Further important information can be derived from the influence exerted on the melting behavior of the PA6 granules by the melt temperatures of the extrudate measured at the individual removal points. Figure 8 shows the melting behavior of one test series, by way of example, specifying the melt temperatures.

When the speed is varied from 300 to 150 min^{-1}, a clear shift is observed in the point at which the PA6 granules completely disappear in the press plates. At a screw speed of 300 min^{-1}, the blend is already fully melted at SP3. The temperature profile of the melt reveals a temperature in excess of the crystalline melting temperature of PA6 ($T_{K,\mathrm{PA}}$ = 223°C). In other words, the measured melt temperatures back up the statement that full-scale melting takes place early at a speed of 300 min^{-1}. In the further course of the press-plate series, a speed reduction is seen to result in a lower melt temperature profile over the length of the melting section, and the point at which the PA6 granules have fully melted shifts toward the screw tip. At a speed of 150 min^{-1}, the temperature of the melt as a whole at SP2 is even below the crystalline melting point of PA6 because of the reduced heat of dissipation. On the basis of the recorded images of the press plates, this behavior is evident from a nonregistratable reduction in the number of PA6 particles between SP2 and SP3. The direct influence of the melt temperature is thus clear, and any breakup of the PA6 granules due to mechanical forces can obviously be neglected. Other influencing variables were also examined in addition to the speed variation. When the throughput is increased, the point at which the PA6 granules are fully melted is similarly seen to shift toward the screw tip. No significant influence is evident when the percentage of disperse PA6 phase is varied (5, 10, 20, and 30% PA6).

Morphology Development

As the low-dose PA6 granules are melting, a very finely dispersed morphology is already developing in parallel to this in the melting section. This phenomenon confirms assumptions from refs.[14–16] and occurred in all the studies conducted in this work. Figure 9 shows the particle size development at the test point used for describing the melting behavior.

A very finely dispersed morphology (ECD$_Z$ = 2.2 μm) has already formed at SP2. Observing the low degree of melting in the press plates from Figure 6 once more, we can assume that these finely dispersed melt drops have formed through the removal of the melt film developing at the granule interfaces. More detailed descriptions of this phenomenon may be found in Potente et al.[14] Further along the melting section, a slight rise occurs in ECD$_Z$, which can be explained *inter alia* by the increased tendency toward coalescence because an increasing number of melt drops develop from the disperse phase as melting progresses.

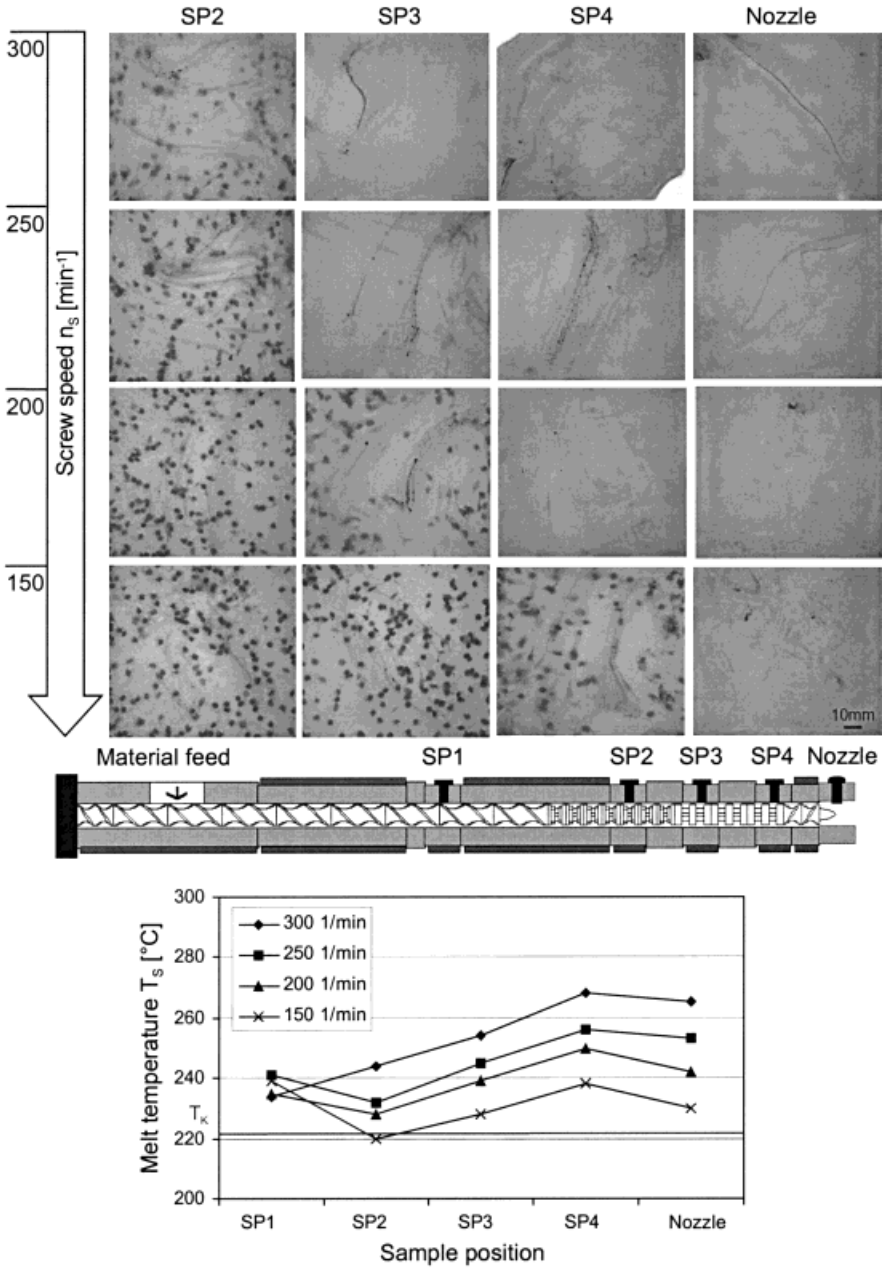

Figure 8 Press-plate series for demonstrating the melting behavior with screw S2, n_S = 300–150 min^{-1}, $\dot{m}$ = 30 kg/h, and w_{PPN} = 90%.

Taking the melting profile from Figure 6 again, we see complete melting occurs between SP3 and SP4. As has already been described, the melting of the granules takes place very rapidly. It is possible to distinguish between two steps here, in accordance with the statements made in the Melting Behavior section. In the first step, a fine film of melt forms around the circumference of the granules as a result of the mechanisms already described. This is scraped off by the melt of the continuous phase that has already formed and is then distributed as a finely dispersed phase. The second step is evidently characterized by very rapid, full-scale melting of the granules. It is thus necessary to have thermal and, more importantly, mechanical conditions that will promote rapid melting of this type. These constraints similarly mean that the PA6 melt that forms breaks down into very fine particles, regardless of the geometric shape in which it occurs (e.g., threads).

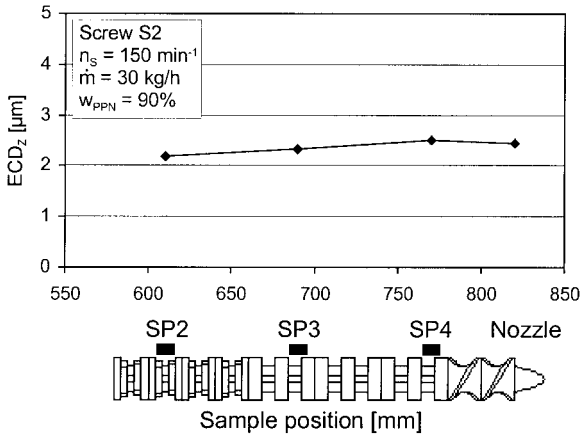

Figure 9 Particle size development with screw S2, n_S = 150 min^{-1}, $\dot{m}$ = 30 kg/h, and w_{PPN} = 90%.

Influence of the Content of the Disperse Phase

It is the content of the disperse phase that has the clearest influence on morphology development. Clear differences in particle size are particularly evident between the test points studied on the profiles set out in Figure 10.

Larger particle diameters are to be found as the disperse-phase content increases, as already shown for the melt-conveying section in Potente et al.[9] Taking Figure 10, we measured an ECD_Z value of 1.2 μm with 5% (by mass) PA6 and an ECD value of 3.8 μm with 30% (by mass) PA6. This considerably higher mean particle diameter can be explained by the higher tendency to coalesce. This, in turn, is promoted by an increasing disperse-phase content and the higher number of particles—or greater volume—of the disperse phase. One particularly striking aspect is that very small particles form alongside very big particles with a high disperse-phase content. This is clear from Figure 11, with the SD taken as a measure of the scatter.

Figure 11 shows that, with a PA6 component of 5% (by mass), ECD_V is only slightly larger than ECD_Z. The SD shows only a very low scatter in the particle diameter. With a PA6 component of 30% (by mass), the picture is completely reversed. The volume-average component deviates greatly from the number-average component, and the SD reveals wide scatter in the particle diameter. Figure 12 shows the frequency distribution, divided into classes, for a varied disperse-phase content. The number of particles evaluated is additionally set out on the z axis of the diagrams, together with the ECD_Z and SD values of all the measured particles for the individual test points. When the content of the disperse phase is increased, the frequency distributions show a clear shift in the

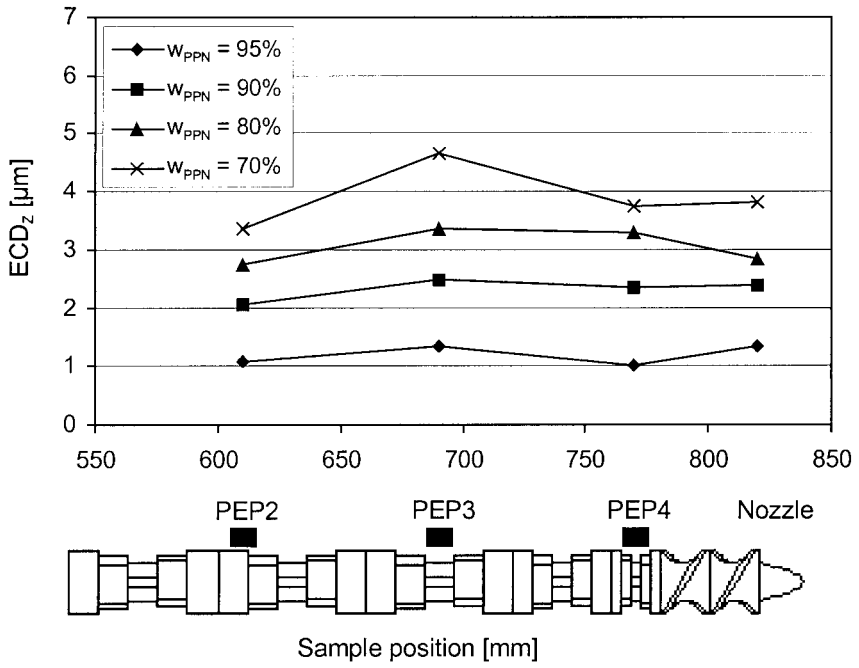

Figure 10 Comparison of the morphology development with changes in the mass of the disperse phase at screw S1, n_S = 300 min^{-1}, $\dot{m}$ = 30 kg/h, and w_{PPH} = 95–70%.

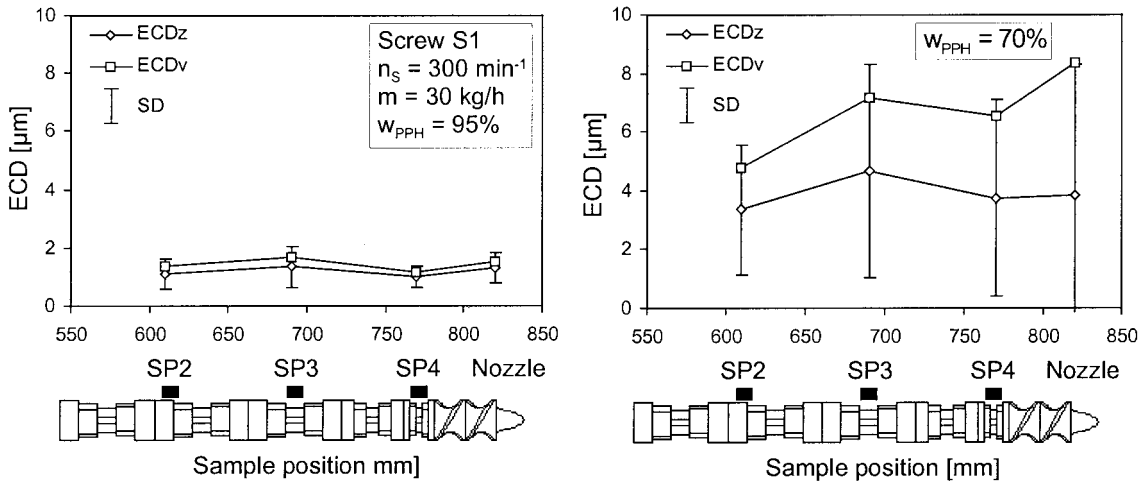

Figure 11 Illustration of the SD and ECD.

particle size toward a broader distribution, supporting the statement in Figure 11.

Influence of the Screw Speed

As is clear from Figure 13, a speed reduction tends to lead to a finer morphology at the screw tip. Only the curve for a speed of 200 min^{-1} shows deviating behavior. If the speed is reduced, particle shear will also be reduced, whereas the residence time in the melting section increases (for the same melt throughput). This produced a finer morphology with the blend system and configura-

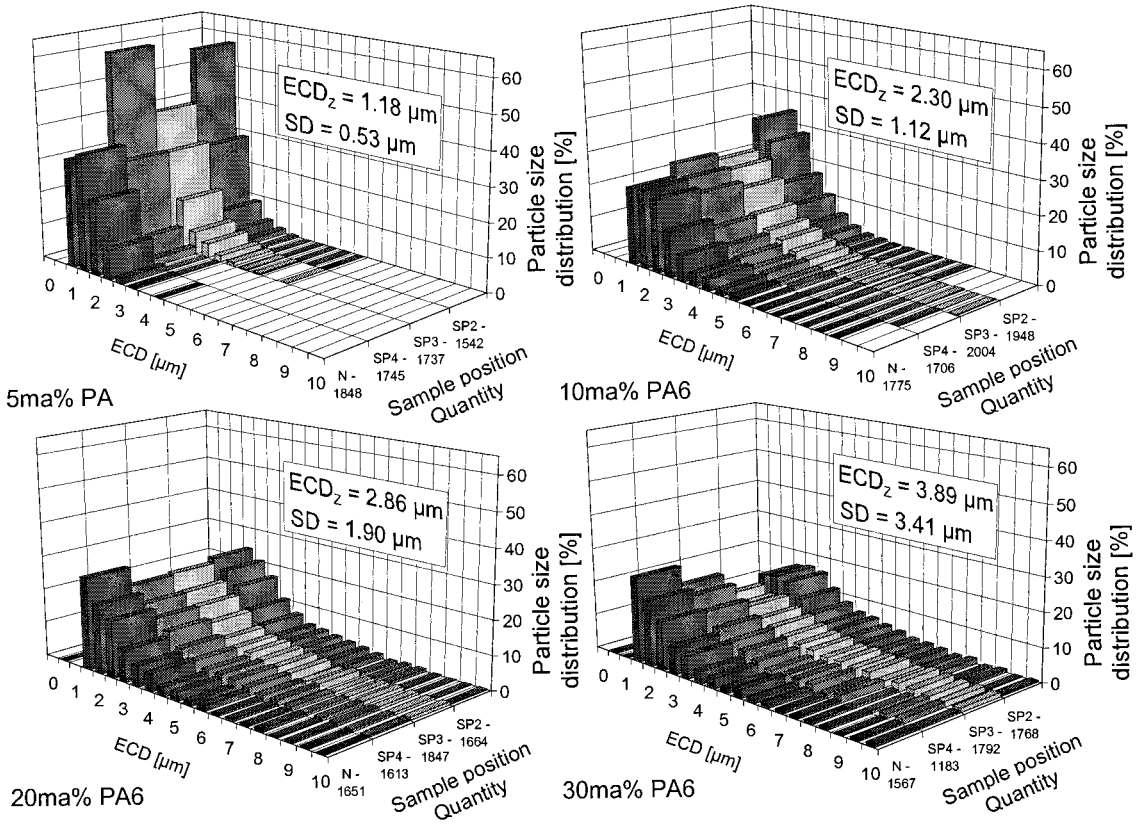

Figure 12 Comparison of the morphology development with variations in the content of the disperse phase at different sample positions with screw S1, n_S = 300 min^{-1}, $\dot{m}$ = 30 kg/h, and w_{PPH} = 95–70%.

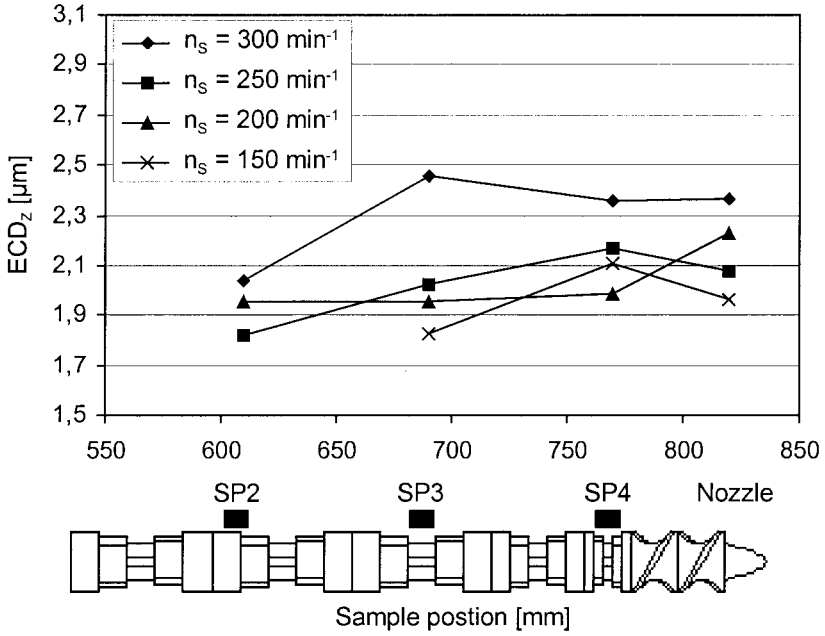

Figure 13 Comparison of the morphology development with changes in the screw speed at screw S1, n_S = 300–150 min^{-1}, $\dot{m}$ = 30 kg/h, and w_{PPH} = 95–70%.

tion employed and tallies with the results for behavior in the melt-conveying section described in the literature.[9,10,16]

Influence of the Mass Throughput

When the mass throughput is varied, a tendency toward smaller particle sizes is evident with an increased mass throughput. With just the morphology at the screw tip observed, a finer morphology results at this point with an increased throughput on all the samples measured, as shown in Figure 14.

If the histograms of the particle size development in Figure 15 are observed, a pronounced shift in distribution toward smaller particle sizes is evident with an increased mass throughput.

This shift in the frequency distribution toward smaller particles as the throughput increases is, in turn, an indicator of very small particles forming both as the disperse phase is fully melting and shortly afterward. If melting behavior is observed for a throughput of 60 kg/h on the press-plate pictures shown in Figure 16, then the PA6 particles are seen to melt at a very late stage, with the particles visible as dark spots. There are even nonmolten PP pellets at removal point SP2, recognizable from the white spots.

PA6 only undergoes complete melting between the final two removal points (SP4 to the die). Coalescence processes can, therefore, have only a minor effect on the morphological structure, and the particle size distribution displays a correspondingly higher number of smaller particle sizes with respect to a throughput of 30 kg/h.

The frequency distribution at the die shown in isolation in Figure 17 clearly confirms the aforementioned effect.

Increasing the throughput from 30 to 60 kg/h causes a rise in the percentage of smallest particles measured (1 μm $<$ ECD $<$ 1.5 μm) from approximately 20 to about 40%, and only small quantities of particles with ECD $>$ 5 μm are seen.

Influence of Viscosity Ratio p

Potente et al.[9] conducted investigations in the melting range with the same blend system and established a slight correlation between the mean particle diameter and the different p values. This correlation can be confirmed with Figure 18.

Although the mean particle diameter still has a value of 1.2 μm for a 5% disperse-phase content with the highly viscous matrix material, it rises to 2.2 μm for this same disperse-phase content with the low-viscosity matrix material. A somewhat less pronounced influence is seen with a 10% disperse-phase content. In this case, the mean particle diameter is 2 μm for the high-viscosity ma-

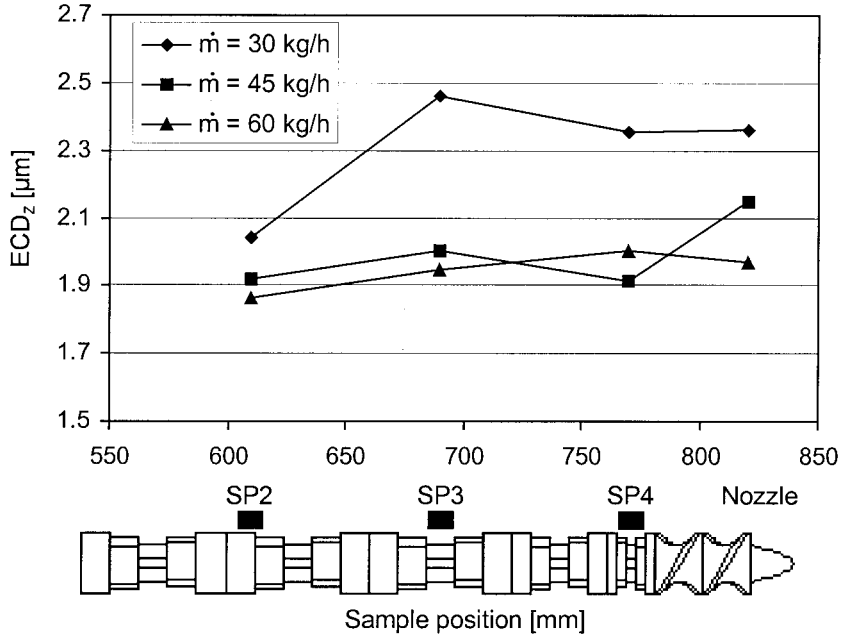

Figure 14 Comparison of the morphology development with changes in the mass throughput at screw S1, n_S = 300 min^{-1}, $\dot{m}$ = 30–60 kg/h, and w_{PPH} = 90%.

trix material and 2.5 μm for the low-viscosity material.

This effect can be explained by the p value of the blend components employed. Drop breakup is essentially described by two dimensionless characteristic values. These are p and the capillary number [Ca; eq. (6)]. Ca constitutes a measure of the drop deformation:

$$\mathrm{Ca} = \frac{\eta_m \dot{\gamma} D}{2\sigma} \tag{6}$$

where D is the droplet diameter. As already mentioned, the results of investigations by Wu et al.[8] showed that p values of 0.1–1 were best for drop breakup. The material combination with the high-viscosity matrix material is thus better suited to drop breakup processes than the one with the low-viscosity matrix material.

The frequency distribution in Figure 19 shows a shift toward larger particle diameters for a low-viscosity matrix material with respect to a high-viscosity matrix material for otherwise identical parameter settings.

Influence of the Screw Design

Figure 20 compares the screw configurations on the basis of variations in the disperse-phase content. It must be remembered that the flow restrictor at the screw tip ensures virtually identical back-pressure behavior in both screw configurations. This greatly influences parameters that would otherwise adjust automatically (pressure, temperature, degree of filling, etc.).

In the curve profiles in Figure 20, no significant differences are evident in the mean particle size for the two screw configurations with the process parameters and blend system employed. Here again, however, the considerable influence of the material combination used is clear. A higher PA6 content leads to a coarser morphology, as discussed in the previous section. The statements made for screw S1 can thus be transposed to the processes taking place in screw S2. The frequency distribution in Figure 21 shows only slight differences between the two screw configurations, as with the ECD curve.

Observed Breakup Mechanisms

The breakup mechanisms were observed on the basis of separated PA6 particles. It can be ascertained in general terms that all the familiar drop breakup mechanisms occurred, such as tip streaming, end pinching, dripping, and folding, along with thread breakup due to sinusoidal cap-

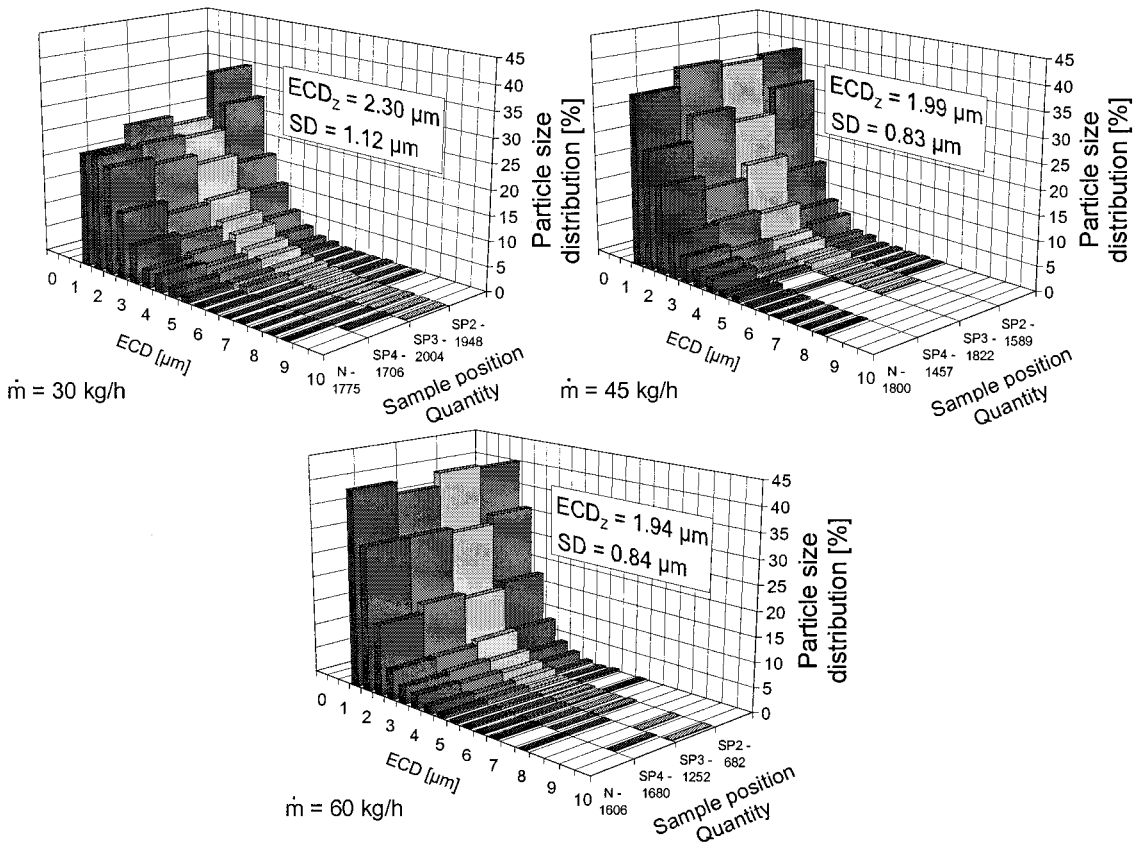

Figure 15 Particle size distribution with changes in the mass throughput at screw S1, n_S = 300 min^{-1}, $\dot{m}$ = 30–60 kg/h, and w_{PPH} = 90%.

illary waves and necking. It is now shown how the morphology develops on a general basis as a result of the aforementioned breakup mechanisms. Samples were cut out of the press plates, and the continuous phase dissolved. Figure 22 shows morphology formation in a PP/PA6 blend when the viscosity of the high-dose PP phase is varied. Figure 22(a) shows the morphology development with a PPH [zero viscosity (η_0) = 11,690 Pa s]. Pronounced thread formation is seen here when melting starts at SP2, with the threads breaking up into very small drops over the remainder of the melting section.

Figure 22(b) shows the morphology development for a PPN (η_0 = 2157 Pa s). In contrast to the morphology development observed previously for PPH, no thread formation is evident here. The pictures show primarily spherical particles with a diameter that does not essentially vary. If the statements made in the Materials section are borne in mind (i.e., when the high-viscosity matrix material is used, a more favorable p drop

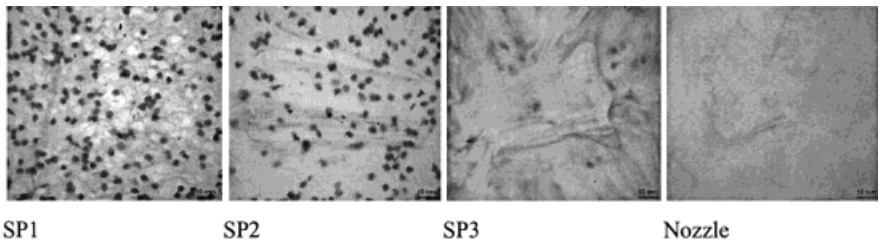

Figure 16 Press-plate series for estimating the melting behavior at screw S1, n_S = 300 min^{-1}, $\dot{m}$ = 60 kg/h, and w_{PPN} = 90%.

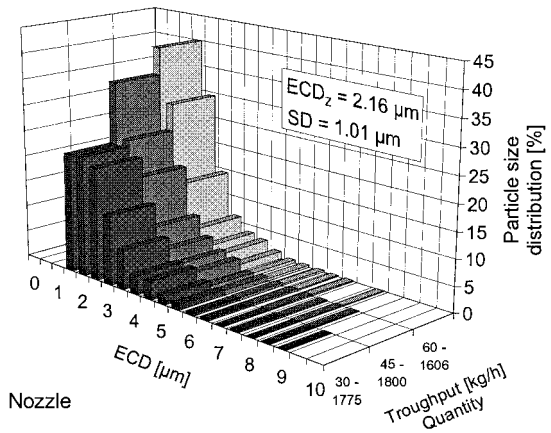

Figure 17 Particle size distribution with changes in the mass throughput at screw S1, nozzle, n_S = 300 min^{-1}, $\dot{m}$ = 30–60 kg/h, and w_{PPH} = 90%.

breakup process prevails), this is confirmed by the long, stretched threads in Figure 22(a). As already specified in the Influence of the Viscosity Ratio section, a finer morphology develops when the higher viscosity matrix material is used. When the lower viscosity matrix phase is used, other breakup mechanisms, such as necking, must play a major role. This leads to a less fine morphology than drop breakup through thread formation according to Ottino.[18]

CONCLUSIONS

We have found that the granule melting process and the finely dispersed morphology that results in the PA6 phase can be described by two processes running in parallel. A finely dispersed morphology forms as soon as melting starts (1.0 μm $< ECD_Z <$ 4.1 μm) and experiences only insignificant change over the length of the melting section. The development of these very small particles can be attributed to the thin layer of melt being scraped off the granule interface where it has formed. The process taking place in parallel is characterized by the very rapid disappearance of the granules and subsequent breakup of the resultant drops of melt into a finely dispersed morphology. The number of pigmented and nonmelted PA6 granules surrounded by PP melt decreases very rapidly over the length of the melting section. The greater the margin is by which the crystalline melting point of PA6 is exceeded, the fewer PA6 particles are found. To permit a quantitative assessment of the morphology, we took samples online at the different SPs, and the microrheological morphology state of the samples was frozen in by quenching of the samples in liquid nitrogen. The disperse-phase content has the clearest influence on morphology. When the PA6 content is increased, the mean ECD of the

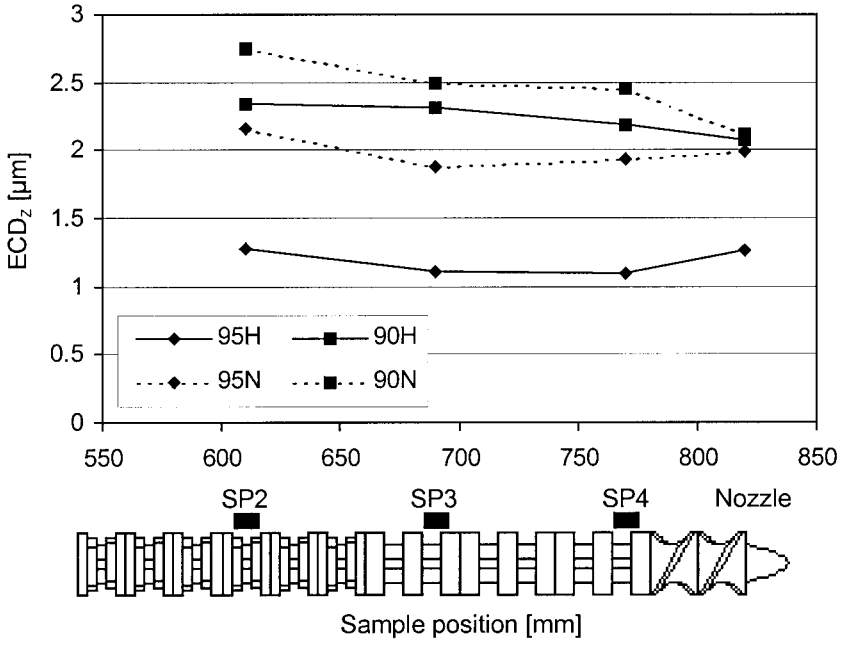

Figure 18 Comparison of the morphology development with changes in the matrix viscosity at screw S2, n_S = 300 min^{-1}, $\dot{m}$ = 30 kg/h, and $w_{PPH,N}$ = 90%.

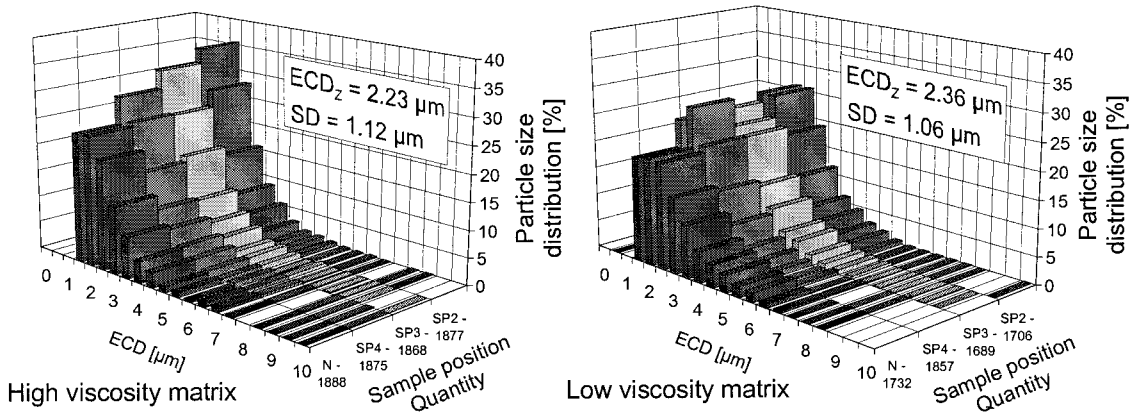

Figure 19 Particle size distribution with changes in the matrix viscosity at screw S2, n_S = 300 min^{-1}, $\dot{m}$ = 30 kg/h, and $w_{\mathrm{PPH,N}}$ = 90%.

particles shifts toward larger particles. When the speed is varied, no direct causal relationship can be established. There is simply a tendency for a lower speed to lead to a finer morphology. If the throughput is increased and a higher viscosity matrix material is employed, a finer morphology will develop. No correlation can be established between the morphology and the screw configuration. Once the blend has completely melted, it is no longer possible for a finer morphology to form under the framework conditions that prevail. Instead, a coarser morphology develops, on account of coalescence processes among other things. A comparison of separated PA6 particles showed that, when PPH was used, pronounced thread formation occurred in PA6 as the disperse phase started to melt. When PPN was used, there was no thread formation but rather almost spherical particles in all cases. The evaluation method of cutting and dissolving out the disperse particles

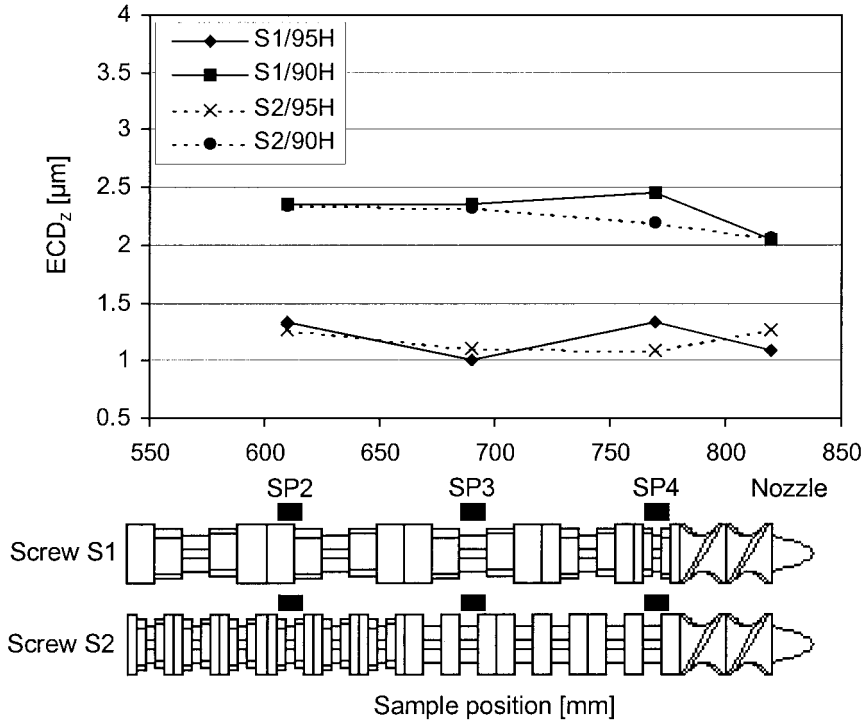

Figure 20 Comparison of the morphology development with changes in the screw design at screw S1/S2, n_S = 300 min^{-1}, $\dot{m}$ = 30 kg/h, and w_{PPH} = 95–90%.

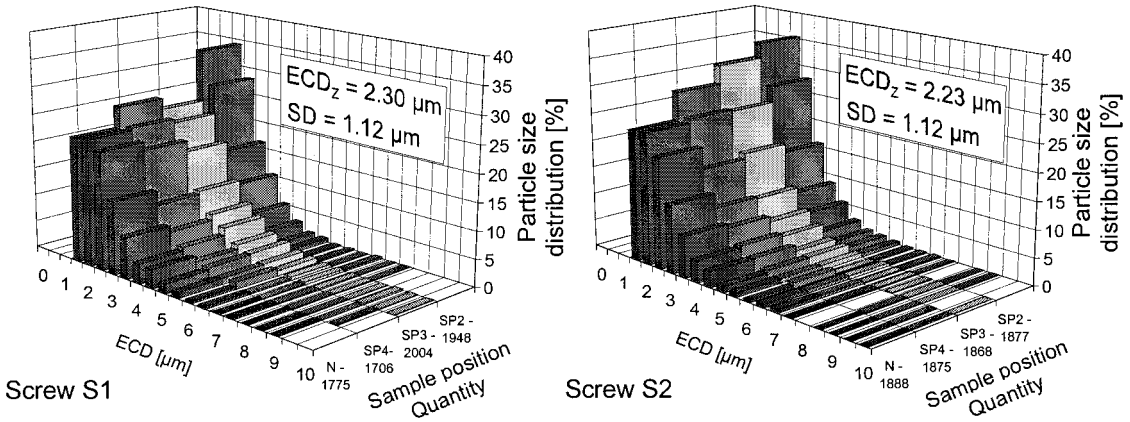

Figure 21 Frequency distribution with changes in the screw design at screw S1/S2, $n_S = 300\ \text{min}^{-1}$, $\dot{m} = 30$ kg/h, and $w_{\text{PPH}} = 90\%$.

must thus be viewed critically because when the thread structures are cut, they give the optical impression of a cut spherical particle, thereby falsifying the evaluation of the particle size.

The results of this research were collated in the framework of projects kindly sponsored by the Deutsche Forschungsgemeinschaft. The authors thank Coperiou Werner & Pfleiderer GmbH for its generous provision

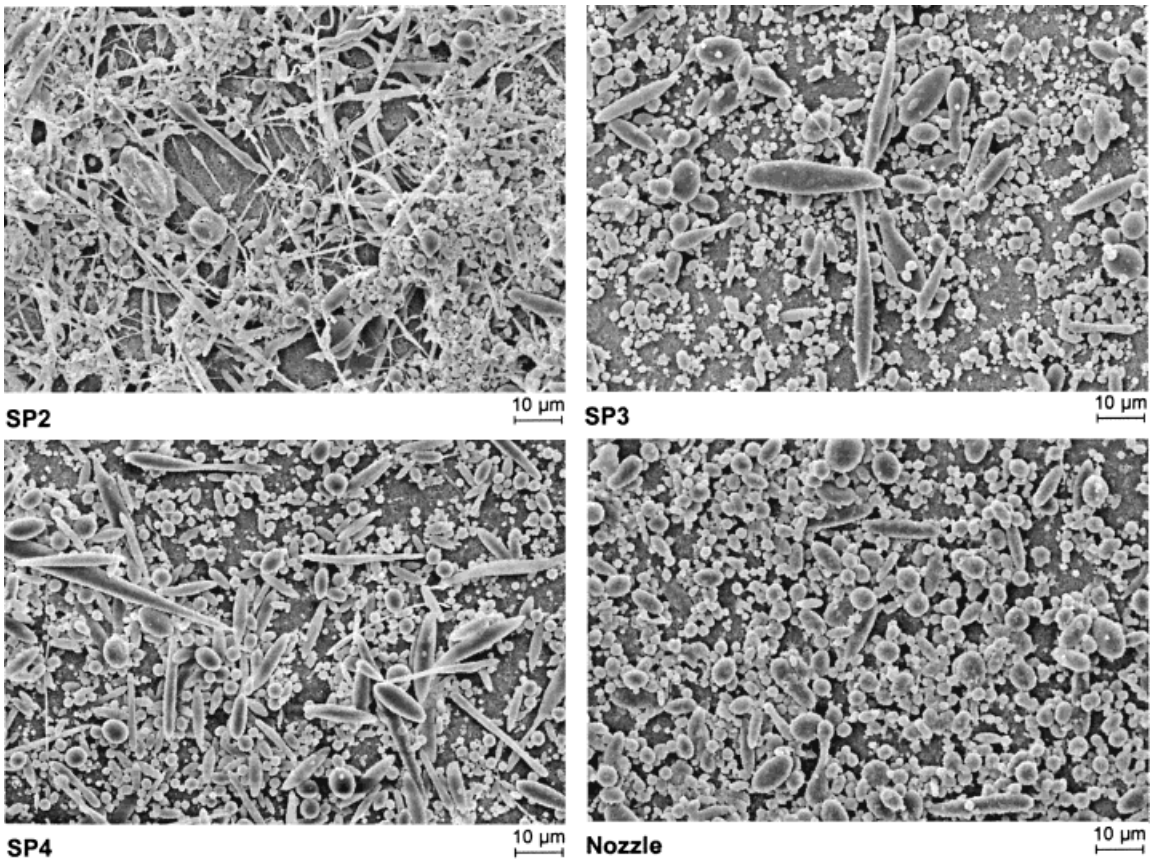

(a)

Figure 22 Separated PA6 particles over the melting section of the extruder with (a) PPH and (b) PPN.

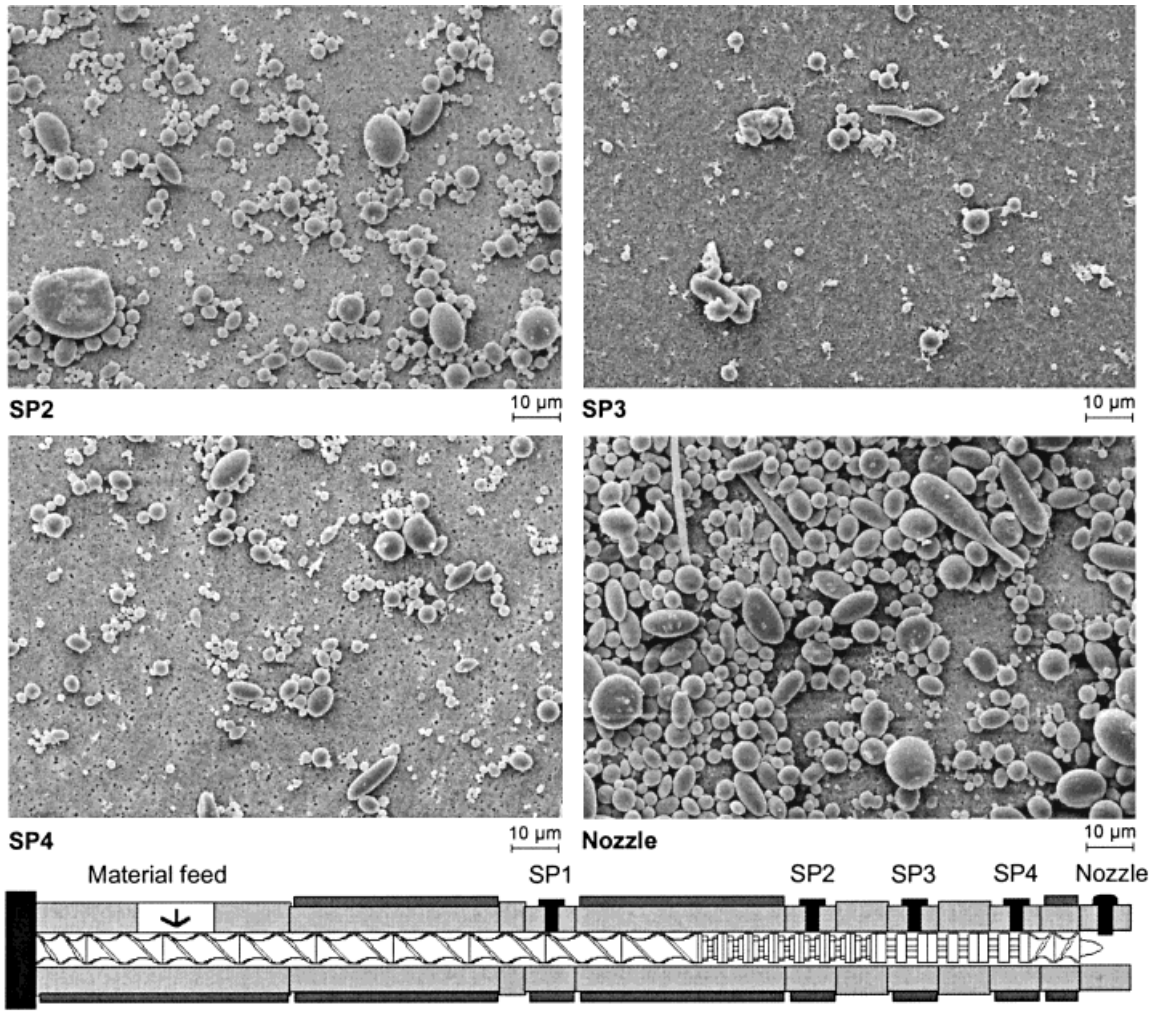

(b)

Figure 22 (*Continued from the previous page*)

of the test extruder and BASF AG and Targor GmbH for their provision of the test materials.

NOMENCLATURE

Ca	capillary number
D	droplet diameter
E	enlargement
ECD	equivalent circle diameter
ECD_V	volume-average particle diameter
ECD_Z	number-average particle diameter
SD	standard deviation
$\dot{m}$	mass throughput
n_S	screw speed
p	viscosity ratio
T_P	press temperature
$T_{K,PA}$	melting temperature of PA6
$T_{K,PP}$	melting temperature of PP
$w_{PPH,N}$	weight content of PPH,N
$\dot{\gamma}$	shear rate
σ	interfacial tension
η_d	viscosity of the disperse phase
η_m	viscosity of the matrix phase

REFERENCES

1. Utracki, L. A. Polym Eng Sci 1995, 35, 2.
2. Todd, D. Compounding in Twin-Screw Extruders in Two-Phase Polymer Systems; Hanser: Munich, 1998.
3. Sundararaj, U.; Dori, Y.; Macosko, C. W. Polymer 1995, 36, 1957.

4. Scott, C. E.; Macosko, W. Polymer 1995, 36, 461.
5. Bawiskar, S.; White, J. L. Int Polym Proc 1995, 10, 105.
6. Lee, S. H.; Bawiskar, S.; Cho, J. W.; White, J. L. Melting and Mixing in Modular Co-Rotating Twin Screw Extruders for Single and Two Component Polymer Systems; PPS 14; Yokohama, Japan, 1998.
7. Grace, H. P. Chem Eng Commun 1982, 14, 225.
8. Wu, S. Polym Eng Sci 1987, 27, 335.
9. Potente, H.; Bastian, M.; Gehring, A.; Stephan, M.; Pötschke, P. J Appl Polym Sci 2000, 76, 708.
10. Essegir, M.; Yu, D. W.; Gogos, C. G.; Todd, D. B. ANTEC 1997.
11. Geng, X.; Zhu, L. ANTEC 1999.
12. Busby, F.; McCullough, T. W.; Hughes, K. R.; Kirk, R. O. ANTEC 1996.
13. Potente, H.; Melisch, U. Int Polym Proc 1996, 11, 29.
14. Potente, H.; Bastian, M.; Bergemann, K.; Senge, M.; Scheel, G.; Winkelmann, Th. Polym Eng Sci, to appear.
15. Bourry, D.; Favis, B. D. Polymer 1998, 39, 1851.
16. Lee, K. J.; Han, C. D. Polymer 2000, 41, 1799.
17. Luciani, A.; Jarrin, J. Polym Eng Sci 1996, 36.
18. Ottino, J. M. Phys Fluids A 1991, 3, 1417.
19. Janssen, J. M. H. Ph.D. Thesis, TU Eindhoven, 1993.